

# Lifetime Constraints for Late Dark Matter Decay

Nicole F. Bell, Ahmad J. Galea and Kalliopi Petraki

School of Physics, The University of Melbourne, Victoria 3010, Australia

We consider a class of late-decaying dark-matter models, in which a dark matter particle decays to a heavy stable daughter of approximately the same mass, together with one or more relativistic particles which carry away only a small fraction of the parent rest mass. Such decays can affect galactic halo structure and evolution, and have been invoked as a remedy to some of the small-scale structure-formation problems of cold dark matter. There are existing stringent limits on the dark matter lifetime if the decays produce photons. By considering examples in which the relativistic decay products instead consist of neutrinos or electron-positron pairs, we derive stringent limits on these scenarios for a wide range of dark matter masses. We thus eliminate a sizable portion of the parameter space for these late-decay models if the dominant decay channel involves Standard Model final states.

PACS numbers: 95.35.+d, 95.85.Pw, 98.62.Gq, 98.70.Vc

## I. INTRODUCTION

Despite the ample gravitational evidence for the existence of dark matter (DM), its nature remains unknown. A promising strategy for identifying the dark-matter particle is to search for a signature produced by DM decay or annihilation, inside the Galactic halo or at cosmological distances. Although such a signature has not yet been identified, the observed radiation backgrounds have served to constrain various decay and annihilation channels [1–13]. In many cases, this has resulted in stringent limits on specific DM candidates.

In this paper we derive constraints for a class of models in which DM decays dominantly via the process

$$\chi \rightarrow \chi' + l, \quad (1)$$

where  $\chi'$  is a massive stable particle, and  $l$  denotes one or more light (or possibly massless) particles. Such decay modes have been discussed in Refs. [14–19]. We focus on the case where the mass splitting between the unstable parent  $\chi$  and the daughter particle  $\chi'$  is small,

$$\Delta m = m_\chi - m_{\chi'} \equiv \varepsilon m_\chi, \quad (2)$$

where  $\varepsilon \ll 1$ . Since the decay replaces an  $\chi$  DM particle with an  $\chi'$  DM particle of approximately the same mass, it does not change the DM energy density significantly and it is thus not constrained to occur at time scales much larger than the age of the Universe. This is quite different from decaying DM scenarios in which the entire energy of the DM is converted into relativistic species during the decay, such as the model of Ref. [20]. The latter scenario is stringently constrained by the cosmic microwave background anisotropies, which set a lower limit on DM lifetime of 123 Gyr at  $1\sigma$  confidence level [21]. The DM decay models we consider in this paper, in which most of the energy is retained in the form of nonrelativistic matter, may be most effectively constrained by comparing the flux of the light particle(s)  $l$  emitted in the decay against the observed radiation backgrounds.

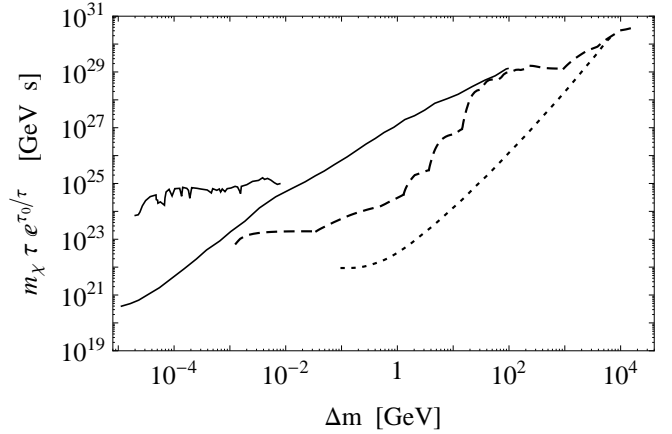


FIG. 1: Constraints on the dark-matter decay channels: (i)  $\chi \rightarrow \chi' + \gamma$ , using the  $\gamma$ -ray line emission limits from the Galactic center region and the isotropic diffuse photon background (irregular and smooth solid lines, respectively) [1]; (ii)  $\chi \rightarrow \chi' + e^- + e^+$  (dashed line); (iii)  $\chi \rightarrow \chi' + \nu + \bar{\nu}$  (dotted line). The regions below the lines are excluded.

An interesting feature of this class of models is that they offer a possible solution to some of the discrepancies between galactic observations and small-scale structure predictions of cold dark matter (CDM) simulations. In CDM simulations, clustering proceeds hierarchically, in a “bottom-up” fashion, resulting in rich structure at small scales. Several disparities with galactic observations have been identified [22–35]. For the disagreement to be resolved within the CDM paradigm, some mechanism that modifies the standard CDM structure-formation picture is necessary. If dark matter decays according to Eq. (1) at time scales comparable to the age of the Universe, the kinetic energy acquired by the heavy daughter,  $\chi'$ , will effectively heat up the dark-matter haloes, and cause them to expand. This can alleviate two of the most glaring CDM problems, the cuspy density profiles of dark-matter haloes and the over-prediction of satellite galaxies [14–

19].

Yüksel and Kistler [1] obtained bounds for the decay channel  $\chi \rightarrow \chi' + \gamma$ , using observations by SPI, COMPTEL and EGRET. Since photons are the most easily detectable particles of the Standard Model (SM), these bounds constrain late-decaying DM scenarios in the most stringent fashion. However, the branching ratio for direct photon production may be tiny in many models. In this paper we investigate DM decay modes to other possible SM particles. We focus on two cases: when the light daughter particles  $l$  produced in the decay are a pair of the lightest charged leptons of the SM

$$\chi \rightarrow \chi' + e^- + e^+, \quad (3)$$

or a pair of the least detectable stable SM particles

$$\chi \rightarrow \chi' + \nu + \bar{\nu}. \quad (4)$$

Given that photons provide the most stringent bounds, and neutrinos the least stringent, our results, together with those of [1], span the full range of constraints for all SM final states. Moreover, constraining the decay into neutrinos places a general lower bound on the DM lifetime for decay to *any* SM particle.

The production of electrons and positrons by dark-matter decay can be constrained both by the observed positron flux and by the observed photon background. Electrons and positrons propagate in the Galaxy and produce photons in a variety of ways. We consider a comprehensive list of effects which result in photon emission associated with the dark-matter decay into  $e^\pm$  pairs, including inverse Compton scattering, bremsstrahlung, synchrotron radiation, in-flight and at-rest annihilations and internal bremsstrahlung. We compare the expected signals with data from Fermi LAT, COMPTEL, EGRET and INTEGRAL. The decay into  $\nu\bar{\nu}$  can be constrained by the atmospheric-neutrino background, and by data from the Super-Kamiokande search for the diffuse supernova neutrino background.

In Sec. II we derive the constraints on the decay channels (3) and (4). We present our results in Fig. 1, together with the constraints derived in Ref. [1] for decay to a photon. In Sec. III, we investigate whether these limits permit DM decay to have a significant effect on the formation of galactic structure. We focus on late-decay scenarios, at times  $\gtrsim 0.1$  Gyr, in accordance with the work of Refs. [16–19]. For the decay modes described in Eq. (3), and Eq. (4), our constraints eliminate a sizable band of the  $\tau$  vs  $m_\chi$  parameter space. However, significant parameter space for which DM decay may influence halo structure remains available. In Sec. IV we turn our attention to models which are not necessarily motivated by the structure formation debate, nevertheless they involve decay of a relic population of particles into states of similar mass. In such models, the decaying particles may amount only to a small fraction of the total DM density of the Universe. We explore the applicability of our constraints on these scenarios and comment on specific particle-physics models.

## II. CONSTRAINTS ON DARK-MATTER DECAY

The energy of the light particles produced in the decays depends on the mass splitting between the parent and the heavy daughter particle,  $\Delta m$ . Their flux is inversely proportional to the lifetime,  $\tau$ , and the mass,  $m_\chi$ , of the parent particle. The latter determines the number density of the DM particles. Observations thus set a lower limit on the product  $m_\chi\tau$  as a function of  $\Delta m$ .

However, if  $\tau$  is comparable to the age of the Universe  $\tau_0 \sim 13$  Gyr, an essential element in the proposed late-decaying DM resolutions of the small-scale structure problems of CDM [16–19], the abundance of  $\chi$  particles may have changed significantly due to decay. Observational bounds should then be cast in the form  $m_\chi\tau e^{\tau_0/\tau} \geq \mathcal{F}(\Delta m)$ , reflecting the exponential suppression of the parent-particle number density today. (The observational bound,  $\mathcal{F}(\Delta m)$ , is presented in Fig. 1 and will be discussed further below.) Note that for sufficiently short lifetime,  $\tau \ll \tau_0$ , all the  $\chi$  particles decay to the stable  $\chi'$  state very early on, thus leaving no observational signal in the Universe today, while for sufficiently long lifetimes,  $\tau \gg \tau_0$ , the current decay probability will be very small. The lifetimes of interest to us, i.e., those that we can probe via indirect detection of the DM decay products, lie between these two extremes.

In our analysis below, we will assume that the  $\chi$  particles originally constitute all of the DM, with no significant admixture of the similar-mass  $\chi'$  particles. Comparable initial abundances of  $\chi$  and  $\chi'$  might be anticipated in canonical thermal-relic realizations of such a DM model. However, our limits can easily be rescaled to account for multicomponent DM, and a down-scaling of our constraints by a factor of  $\sim 2$  would not qualitatively affect our conclusions.

The massive daughter particle  $\chi'$  will be produced non-relativistically, provided that  $\Delta m \ll m_\chi$ . Then, to a good approximation, the light particles share the energy  $\Delta m$  released in the decay, such that  $E_1 + E_2 \simeq \Delta m$ , where  $E_1, E_2$  are the energies of the two light leptons. For the 3-body decay channels described in Eq.(3) and Eq.(4), the energy spectra of the daughter particles is in general model-dependent. However, we find that the constraints on the dark-matter decay are rather insensitive to the actual spectrum. We illustrate this by presenting results for two limiting cases of the daughter energy spectra:

- i. Monoenergetic, where the energy spectrum per decay for each light daughter species is

$$dN/dE = \delta(E - \Delta m/2). \quad (5)$$

- ii. Flat, where is spectrum is uniform over the allowed energy range such that

$$dN/dE = 1/(\Delta m - 2m_l), \quad (6)$$

where  $m_l = m_e$  for the decay into  $e^\pm$  and  $m_l = 0$  for the decay into neutrinos.

For each of the decay modes analyzed, we pick the most conservative limits to further continue our discussion<sup>1</sup>.

The constraints on DM decay depend on the DM halo density profile. Although there are uncertainties in the profile, particularly near the Galactic center (GC), we shall see below that these uncertainties are subdominant. For consistency with the results of other analyses which we shall employ in our calculations, we use the Navarro-Frenk-White (NFW) [36] profile throughout. The standard parametrization is

$$\rho(r) = \frac{\rho_0}{(r/r_s)^\gamma [1 + (r/r_s)^\alpha]^{(\beta-\gamma)/\alpha}}, \quad (7)$$

where  $(\alpha, \beta, \gamma) = (1, 3, 1)$ . For the Milky Way  $r_s = 20$  kpc, and the normalization  $\rho_0$  is fixed such that at the solar-circle distance  $R_{\text{sc}} = 8.5$  kpc, the density is  $\rho(R_{\text{sc}}) = 0.3 \text{ GeV cm}^{-3}$ .

### A. Decay into electrons and positrons.

Electrons and positrons injected in the Galaxy will produce photon fluxes spanning a wide range of energies, by a variety of different mechanisms. The injection rate can thus be constrained by the resulting contribution to the Galactic photon backgrounds. We will also derive constraints based upon direct detection of positrons. Below, we describe the methods used to estimate the signal produced by each effect. We present the resulting constraints in Fig. 2.

#### 1. Internal bremsstrahlung.

Electromagnetic radiative corrections to the DM decay channel to charged particles inevitably produce real  $\gamma$  rays. If the process  $\chi \rightarrow \chi' + e^\pm$  takes place, then  $\chi \rightarrow \chi' + e^\pm + \gamma$  must also take place since either one of the final state charged particles can radiate a photon. This process is called internal bremsstrahlung (IB). Note that the photon in the IB process arises directly in the Feynman diagram for the decay, and is unrelated to regular bremsstrahlung which results from interaction in a medium. Importantly, the IB spectrum and normalization is approximately model-independent. In addition, as the IB photon flux does not depend on the propagation of charged decay products in the Galaxy, it is free of

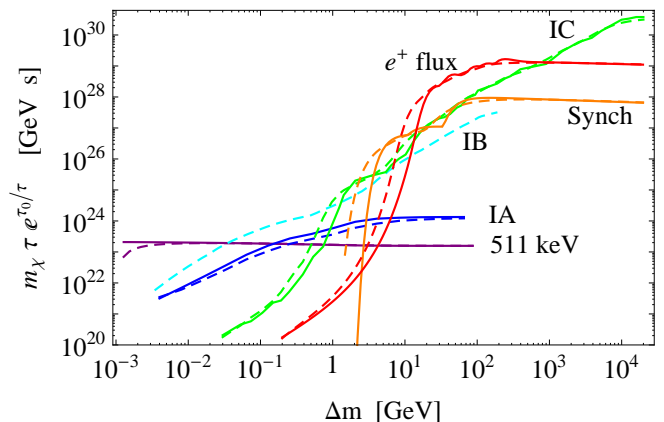


FIG. 2: Limits on dark-matter decay process  $\chi \rightarrow \chi' + e^- + e^+$ , obtained from internal bremsstrahlung (IB, cyan), in-flight annihilation (IA, blue), annihilation at rest (511 keV, purple), inverse Compton scattering and bremsstrahlung emission (IC, green), synchrotron radiation (Synch, orange), and positron flux ( $e^+$  flux, red). Solid lines correspond to a monoenergetic spectrum of electrons and positrons, while dashed lines assume a flat injection spectrum over the allowed energy range. The regions below the lines are excluded.

uncertainties associated with the astrophysical environment. IB is thus a very clean and reliable technique for obtaining limits on DM decay to charged particles, with the only source of uncertainty residing in the DM profile adopted.

The IB differential decay width is [37]

$$\frac{d\Gamma_{\text{IB}}}{dE} = \Gamma \times h(E), \quad (8)$$

where  $E$  is the energy of the photon emitted,  $\Gamma = \tau^{-1}$  is the rate of lowest order decay process  $\chi \rightarrow \chi' + e^\pm$ , and  $h(E)$  is the photon spectrum per  $\chi \rightarrow \chi' + e^\pm$  decay. This spectrum is independent of the new physics which mediates the decay, and is given by

$$h(E) \simeq \frac{\alpha}{\pi} \frac{1}{E} \ln \left( \frac{s'}{m_e^2} \right) \left[ 1 + \left( \frac{s'}{s} \right)^2 \right], \quad (9)$$

where  $s' = s(1 - E/E_{\text{max}})$ , with  $s$  being the energy released in the decay, and  $E_{\text{max}}$  the maximum energy that can be imparted to the radiated photon<sup>2</sup>. In the 3-body decay we consider here,  $s = (\Delta m - 2m_e)^2$ , and  $E_{\text{max}} = \sqrt{s}(1 - \varepsilon/2) \simeq \sqrt{s}$ .<sup>3</sup>

<sup>1</sup> As a consistency check, we verify that for a specific  $\Delta m$ , the limit obtained on  $m_\chi \tau e^{\tau_0/\tau}$  when an extended injection distribution is used, does not exceed the maximum value of this limit obtained for monoenergetic injection for mass splittings up to  $2\Delta m$ , i.e.  $[m_\chi \tau e^{\tau_0/\tau}(\Delta m)]_{\text{ext}} \leq \max_{\mu < 2\Delta m} [m_\chi \tau e^{\tau_0/\tau}(\mu)]_{\text{mono}}$

<sup>2</sup> These general definitions of  $s, s'$  reproduce the correct expressions for the case of annihilation into two charged particles [37] and for muon decay [38].

<sup>3</sup> Note that the phase space available to the photon when one of the decay products is emitted nonrelativistically (i.e. when  $\varepsilon \ll 1$ ) is larger than when all decay products are relativistic (e.g. muon

The shape of the IB photon spectrum is determined by the  $1/E$  factor in Eq. (9), while the logarithmic factor provides a sharp cutoff at  $E \simeq E_{\max}$ . Since the galactic photon background varies approximately as  $E^{-2}$ , the high-energy region of the IB photon spectrum will provide the most stringent constraints.

The flux of photons due to IB will be proportional to the dark matter density integrated over the line of sight. At an angle  $\psi$  from the Galactic center, the line-of-sight integral is

$$J(\psi) = \int_0^{l_{\max}} dl \rho_\chi \left( \sqrt{R_{\text{sc}}^2 - 2lR_{\text{sc}} \cos \psi + l^2} \right), \quad (10)$$

where  $l_{\max} = \sqrt{R_{\text{MW}}^2 - R_{\text{sc}}^2 \sin^2 \psi} + R_{\text{sc}} \sin \psi$ . The average of  $J$  over a cone of half-angle  $\psi$  centered on the GC is

$$\mathcal{J}_{\Delta\Omega}(\psi) = \frac{2\pi}{\Delta\Omega} \int_0^\psi J(\psi') \sin \psi' d\psi', \quad (11)$$

where  $\Delta\Omega = 2\pi(1 - \cos \psi)$ .

The expected photon flux, per unit solid angle, due to IB is then

$$\frac{d\Phi_{\text{IB}}}{dE} = \frac{1}{4\pi} \frac{1}{m_\chi \tau e^{\tau_0/\tau}} \mathcal{J}_{\Delta\Omega} h(E). \quad (12)$$

COMPTEL observations show that the  $\gamma$ -ray background remains approximately constant within  $|l| < 30^\circ$ . Thus, along the Galactic plane, the signal-to-background ratio for IB is maximized at the GC. Here, we will average over the region  $\psi < 5^\circ$ , which exceeds the angular resolution with which both COMPTEL and EGRET data have been reported [39, 40]. The IB limits are shown in Fig. 2 (cyan line).

## 2. In-flight and at-rest annihilations.

Positrons produced by DM decay will propagate in the interstellar medium, lose energy, and annihilate with electrons. Most positrons will survive until they become non-relativistic, and annihilate at rest to produce a 511 keV annihilation line (together with a three-photon continuum). However, a portion of the positrons annihilate in flight while still relativistic. These in-flight annihilations (IA) can produce a significant flux of  $\gamma$  rays [41].

Reference [41] considered the injection of positrons at the Galactic center, and related the flux of IA  $\gamma$ -rays to the flux of 511 keV photons. This was used to derive a

constraint on the injection energy of positrons that contribute to the observed Galactic 511 keV line.

We will follow a similar approach to obtain limits on DM decay into  $e^\pm$ . In our case, however, the overall normalization of the photon flux is not fixed by the observed 511 keV line intensity, but is instead determined by the DM decay rate. The continuum  $\gamma$ -ray flux due to IA, and the 511 keV photons from annihilation at rest, thus yield two separate sets of constraints. The positron injection, deceleration and annihilation budget is described by the equation [42]

$$\frac{\partial n}{\partial t} + \frac{\partial}{\partial \gamma} \left( \frac{d\gamma}{dt} n \right) = -n_H \sigma(\gamma) \beta n(\gamma, t) + \Gamma_{\text{inj}} \frac{dN}{d\gamma}, \quad (13)$$

where  $n(\gamma, t)d\gamma$  is the density of positrons with energy  $\gamma m_e$ , at time  $t$ ,  $\Gamma_{\text{inj}} = \rho_\chi e^{-\tau_0/\tau} / m_\chi \tau$  is the positron-density injection rate due to DM decay, and  $dN/d\gamma$  is the positron spectrum per decay. The positron annihilation cross section  $\sigma(\gamma)$  on electrons at rest is [43]

$$\sigma = \frac{\pi r_e^2}{\gamma + 1} \left[ \frac{\gamma^2 + 4\gamma + 1}{\gamma^2 - 1} \ln \left( \gamma + \sqrt{\gamma^2 - 1} \right) - \frac{\gamma + 3}{\sqrt{\gamma^2 - 1}} \right], \quad (14)$$

where  $r_e$  is the classical electron radius.

At energies lower than  $\sim 1$  GeV, ionization and Coulomb losses (in a neutral or an ionized medium, respectively) dominate over energy loss due to synchrotron, bremsstrahlung and inverse Compton effects, while at higher energies synchrotron losses are more important. The energy loss rates due to ionization, Coulomb scattering and synchrotron emission are [42]

$$\left| \frac{d\gamma}{dt} \right|_i \simeq 4.4 \cdot 10^{-15} \text{ s}^{-1} \left( \frac{n_H}{0.1 \text{ cm}^{-3}} \right) \frac{\ln \gamma + 6.8}{\beta}, \quad (15)$$

$$\left| \frac{d\gamma}{dt} \right|_C \simeq 1.5 \cdot 10^{-15} \text{ s}^{-1} \left( \frac{n_H}{0.1 \text{ cm}^{-3}} \right) \frac{\ln \gamma + 75.9}{\beta}, \quad (16)$$

$$\left| \frac{d\gamma}{dt} \right|_s \simeq 5.4 \cdot 10^{-24} \text{ s}^{-1} \left( \frac{U_B}{0.2 \frac{\text{eV}}{\text{cm}^3}} \right) (\gamma^2 - 1), \quad (17)$$

where  $n_H$  is the hydrogen number density of the medium, and  $U_B = B^2/8\pi$  is the energy density of the magnetic field. Equations (15) and Eq.(16) apply to a fully neutral and or fully ionized medium, respectively. As a conservative choice, we set the ionization fraction of the interstellar gas to be  $x_i \approx 0.51$ . Compared with a completely neutral medium, energy losses in an ionized medium are larger and thus IA constraints weaker, by a factor of a few [44]

As evident from Eqs. (15) and (16), it takes approximately  $10^7$  yr for relativistic positrons to slow down and annihilate. If positron injection (DM decay) has been taking place over a much larger time period,  $\tau > 0.1$  Gyr, the positrons reach a steady-state distribution. The time-independent solution of Eq.(13) is

$$n(\gamma) = \frac{\rho_\chi}{m_\chi \tau e^{\tau_0/\tau}} \frac{1}{\left| \frac{d\gamma}{dt} \right|} \int_\gamma^\infty d\gamma' \frac{dN}{d\gamma'} P_{\gamma' \rightarrow \gamma}, \quad (18)$$

---

decay, where  $\varepsilon \simeq 1$ ). This is because a heavy daughter particle can absorb recoil momentum, without carrying away a significant amount of energy.

where

$$P_{\gamma' \rightarrow \gamma} \equiv \exp \left[ -n_{\text{H}} \int_{\gamma}^{\gamma'} \frac{\sigma(\gamma'') \beta''}{\left| \frac{d\gamma''}{dt} \right|} d\gamma'' \right] \quad (19)$$

is the *survival probability*, introduced in [41], of positrons injected at energy  $\gamma' m_e$  to have not annihilated by the time they reach energy  $\gamma m_e$ .

Here, we have ignored the effects of spatial diffusion of positrons, which would require detailed modeling. This approximation is sufficient provided that the positrons remain trapped within the region we consider<sup>4</sup>. In what follows, we will calculate the expected photon flux due to annihilation in a cylindrical region of radius  $r_{\text{max}} = 3 \text{ kpc}$  and half-height  $z_{\text{max}} = 0.5 \text{ kpc}$ , centered at the GC. This is well inside what is taken to be the diffusion area in most models simulating cosmic-ray propagation in the Galaxy. Because of the Galactic magnetic field, charged particles are largely expected to follow the magnetic lines and converge toward the GC, as long as their Larmor radius,  $r_L = \gamma m / qB$ , is much smaller than the scale of variation of the magnetic field. In the Milky Way,  $B \gtrsim \text{few } \mu\text{G}$ , and  $(d \ln B / dr)^{-1} \sim \text{few kpc}$  [5]. Positrons are thus expected to follow the magnetic lines, even for energies much higher than the ones considered in this analysis. Any influx of positrons in the region under consideration would only lead to more stringent constraints than the ones derived here. (The possibility of transport of the positrons from the disk to the GC has been discussed in detail in [45].)

The diffuse  $\gamma$ -ray background of the Galactic plane has been measured by COMPTEL in the energy range 1–30 MeV for the region  $|l| < 30^\circ$ ,  $|b| < 5^\circ$  (Galactic longitude and latitude, respectively) and by EGRET, in the energy range 30 MeV–30 GeV and the region  $|b| < 10^\circ$  [39, 40]. The cylindrical volume defined above is covered by these observations, and encompassed within a conical patch of solid angle  $\Delta\Omega = 4l_{\text{max}} \sin b_{\text{max}} \simeq 0.13 \text{ sr}$ , with  $l_{\text{max}} = \arcsin(r_{\text{max}}/R_{\text{sc}}) \simeq 20^\circ$  and  $b_{\text{max}} = \arctan[z_{\text{max}}/(R_{\text{sc}} - r_{\text{max}})] \simeq 5^\circ$ . The comparison of the signal from the cylindrical region with the background radiation emanating from the larger conical region, keeps our constraints conservative.

The flux of photons (per unit solid angle) due to IA is

$$\frac{d\Phi_{\text{IA}}}{dk} = \frac{1}{\Delta\Omega} \frac{1}{4\pi R_{\text{sc}}^2} \int dV \int d\gamma n(\gamma) n_{\text{H}} \frac{d\sigma(k, \gamma)}{dk} \beta,$$

<sup>4</sup> Along with spatial diffusion, we also ignore the related effect of reacceleration. This becomes more important with increasing energy, since the diffusion coefficient in momentum space is  $D_{pp} \propto p^{2-\delta}$  with  $\delta < 1$  [5, 6, 42]. However, the probability to annihilate drops sharply at high energies, and thus pumping more energy in already energetic positrons does not affect the IA constraints significantly.

where the spatial integration is over the cylindrical region considered. The differential cross section  $\frac{d\sigma(k, \gamma)}{dk}$  for a positron of energy  $\gamma m_e$  to produce a photon of energy  $E = km_e$  is [41, 46]

$$\frac{d\sigma(k, \gamma)}{dk} = \frac{\pi r_e^2}{\gamma^2 - 1} \left[ \frac{-\frac{3+\gamma}{1+\gamma} + \frac{3+\gamma}{k} - \frac{1}{k^2}}{\left(1 - \frac{k}{1+\gamma}\right)^2} - 2 \right], \quad (20)$$

while the minimum positron energy  $\gamma_{\text{min}} m_e$  required to produce a photon of energy  $km_e$  is given by

$$\gamma_{\text{min}}(k) = k - \frac{1}{2} + \frac{1}{2(2k-1)}. \quad (21)$$

For the steady-state positron distribution  $n(\gamma)$ , given in Eq.(18), the expected  $\gamma$ -ray signal from IA is

$$\frac{d\Phi_{\text{IA}}}{dk} = \frac{1}{m_{\chi\tau} e^{\tau_0/\tau}} \frac{\int dV \rho_{\chi}}{4\pi R_{\text{sc}}^2 \Delta\Omega} \int_{\gamma_{\text{min}}(k)}^{\infty} d\gamma \frac{dN}{d\gamma} \mathcal{Q}(k, \gamma), \quad (22)$$

where

$$\mathcal{Q}(k, \gamma) \equiv n_{\text{H}} \int_{\gamma_{\text{min}}(k)}^{\gamma} d\gamma' \frac{\sqrt{\gamma'^2 - 1}}{\gamma'} \frac{d\sigma(k, \gamma')}{dk} \frac{P_{\gamma \rightarrow \gamma'}}{\left| \frac{d\gamma'}{dt} \right|}. \quad (23)$$

The IA flux of Eq. (22) is compared to the  $\gamma$ -ray background reported by COMPTEL and EGRET [39, 40], and compiled in Ref. [12]. The resulting lower limit on  $m_{\chi\tau} e^{\tau_0/\tau}$  is presented in Fig. 2 (blue line) and increases with increasing  $\Delta m$ , since positrons injected at higher energy spend more time as relativistic, and are more likely to annihilate in flight. However, the annihilation probability diminishes at high energies, which is manifest by the plateau in the lifetime bound for energies  $\gtrsim 3 \text{ GeV}$ .

The majority of positrons survive until they become nonrelativistic. Then, they either annihilate directly with electrons to produce 511 keV photons, or they form a positronium bound state. Positronium subsequently annihilates, with probability 25% into two 511 keV photons, or with probability 75% into a three photon continuum. The positronium fraction in the Galaxy is fixed by the relative intensities of the  $\gamma$ -ray continuum below 511 keV, and the 511 keV line. In our Galaxy  $f = 0.967 \pm 0.022$  [47].

If DM decays into  $e^\pm$  pairs, the flux of 511 keV photons produced is determined, in the steady-state regime, by the rate at which positrons arrive at rest. For each nonrelativistic positron, there will be  $2(1-f) + 2f/4 = 2(1-3f/4)$  photons contributing to the line. The expected flux of 511 keV photons is

$$\Phi_{511} = \frac{2(1-3f/4)}{m_{\chi\tau} e^{\tau_0/\tau}} \frac{\int dV \rho_{\chi}}{4\pi R_{\text{sc}}^2 \Delta\Omega} \int_1^{\infty} d\gamma \frac{dN}{d\gamma} P_{\gamma \rightarrow 1}. \quad (24)$$

The  $\gamma$ -ray observations by INTEGRAL have revealed a 511 keV line emission of intensity  $0.94 \times$

$10^{-3} \text{ ph cm}^{-2} \text{ s}^{-1}$  within an integration region  $|l| < 20^\circ$ ,  $|b| < 5^\circ$  [48]. The average flux per steradian is then  $0.0077 \text{ ph cm}^{-2} \text{ s}^{-1} \text{ sr}^{-1}$ . The limits on DM decay arising from annihilation at rest are presented in Fig. 2 (purple line). They exhibit a very slight negative slope towards increasing  $\Delta m$ , which accounts for the (small) portion of positrons annihilating in-flight when injected at high energies.

The IA constraints are stronger than those for annihilation at rest for average positron injection energies  $\langle E \rangle = \Delta m/2 \gtrsim 80 \text{ MeV}$ . This is considerably higher than the corresponding value of  $\sim 3 \text{ MeV}$  found by an appropriate analysis in Ref. [41]. The latter limit was determined by requiring that the IA  $\gamma$ -rays do not exceed 30% of the observed background, instead of the more conservative 100% adopted here. However, the more important factor in reconciling these two analyses is the different signal regions considered. The analysis in Ref. [41] considered the conical region within a  $\sim 0.37 \text{ kpc}$  radius of the GC, which contains the peak of the 511 keV annihilation signal. This is to be compared to our larger cylindrical volume ( $r_{\text{max}} = 3 \text{ kpc}$ ,  $z_{\text{max}} = 0.5 \text{ kpc}$ ) outlined above. The effect of choosing the larger volume is to make the annihilation-at-rest constraints stronger, with respect to those from IA, than for the choice of a smaller region at the Galactic center. The Galactic center is not the optimal observation region to use in setting an annihilation-at-rest limit, because that is where the observed 511 keV background is highest. In addition to resulting in more sensitive annihilation-at-rest limits, the larger volume also renders us insensitive to possible effects of diffusion.

Notice also that the photon fluxes, Eqs. (22) and (24), are independent of the medium number density  $n_{\text{H}}$ , as long as ionization and Coulomb losses dominate, for  $\Delta m \lesssim \text{few GeV}$ . Since the probability to annihilate at even higher energies is insignificant, the results are rather insensitive to  $n_{\text{H}}$ , as well as  $U_B$ , throughout the energy spectrum.

### 3. Inverse Compton scattering, bremsstrahlung emission, synchrotron radiation.

At high energies IA become rather rare, and electrons and positrons propagating in the Galaxy produce radiation more efficiently via other mechanisms. Gamma rays are produced by bremsstrahlung and inverse Compton (IC) scattering of low-energy photons, with the latter effect yielding the dominant contribution. Synchrotron emission in the Galactic magnetic field gives rise to a radio wave signal.

Zhang et al. [5, 6] calculated the photon spectrum expected if electrons and positrons are injected in the Galaxy by DM decay. They assumed a monoenergetic injection spectrum, and modeled the propagation of  $e^\pm$  in the interstellar medium in detail, including the effects of spatial diffusion, convection, energy loss and reaccel-

eration. They compared the resulting spectrum at Earth with observed backgrounds, and encoded their calculations in *response functions* which can be utilized to obtain constraints when convoluted with the DM decay spectrum of a particular model. Here, we use the response functions derived in Ref. [5] for synchrotron radiation, and in Ref. [6] for IC and bremsstrahlung emission, to obtain constraints for the  $\chi \rightarrow \chi' + e^\pm$  decay process.

The main source of uncertainties in deriving the response functions is poor knowledge of the various astrophysical parameters which determine the propagation of  $e^\pm$  in the Galaxy. The most significant contribution comes from the height of the diffusion zone. The Galactic magnetic field, although also quite poorly known, contributes subdominantly to the total uncertainty. This is true even for the synchrotron response functions, since although the magnetic field may be rather uncertain in the Galactic bulge, the directions which optimize the signal-to-background ratio point away from the GC. Different choices for the DM halo profile have a small influence on the response functions, since the flux is only proportional to the density (as opposed to the  $\rho^2$  dependence applicable for DM annihilation) [5, 6].

The IC and bremsstrahlung emission is constrained by using the Fermi LAT  $\gamma$ -ray maps derived in [49], for the energy range 0.5 GeV–300 GeV. Because of reacceleration, this permits limits for  $e^\pm$  injection energies in a much wider range, 0.01 GeV –  $10^4 \text{ GeV}$ . The strength of the limits, of course, sharply diminishes in the low-energy part of this range. At energies above 50 GeV, the Fermi data may suffer from significant background contamination, while point sources have not been subtracted. These effects lead to more conservative constraints. There are also various astrophysical contributions to the  $\gamma$ -ray flux, such as nucleus-nucleus photoproduction via  $\pi^0$  decay, and IC and bremsstrahlung radiation from cosmic-ray electrons and positrons. In the spirit of setting conservative limits on DM decay, we will use response functions where these foregrounds have not been subtracted. The patch of sky chosen to compare the expected signal to observations is  $|l| < 20^\circ$  and  $-18^\circ < b < -10^\circ$  [6].

The synchrotron response functions derived in Ref. [5] correspond to 408 MHz, 1.42 GHz and 23 GHz sky maps, and yield constraints for  $e^\pm$  injection energies in the range, 0.1 GeV –  $10^4 \text{ GeV}$ . The directions that optimize the signal-to-background ratio are different for each of the sky maps used, and are located close to, but not at, the GC. (Similar sensitivity may be achieved with the isotropic diffuse flux measured by Fermi; see Ref.[50] for relevant limits on the process  $\chi \rightarrow e^\pm$ .)

The response functions reported all assume a NFW halo profile. The expected signal from particles produced by DM decay is compared to observed photon flux including a  $2\sigma$  error. The dependence on the propagation model, for both the synchrotron and the IC plus bremsstrahlung emission, becomes more significant at  $e^\pm$  injection energies lower than about 10 GeV. This is because the limits in that range rely solely on the effect

of reacceleration, which depends strongly on the model adopted, while no actual low-energy background data are used. For the synchrotron constraints, we adopt the “DR” model [5], which yields moderately conservative constraints along the entire energy range. For the IC plus bremsstrahlung constraints we adopt the “L1” model, whose response functions are most comprehensively reported in [6].

The limits on DM decay from IC plus bremsstrahlung radiation and synchrotron emission are shown in Fig. 2 (green and orange lines, respectively).

#### 4. Positron flux.

The DM decay into  $e^\pm$  pairs can be constrained by direct observations of the positron flux on Earth. Utilizing the same propagation models as the ones used for the synchrotron emission, Zhang et al. [5] constructed response functions, comparing the expected positron flux to PAMELA data [51]. The positron fraction reported by PAMELA was converted into positron flux using the  $e^\pm$  total flux observed by the Fermi telescope [52].

The positron-flux response functions are based on observations of positrons in seven energy bands in the range 10.17 GeV – 82.55 GeV. Depending on the model used, they can provide meaningful constraints for positron injection energies within the range 0.1 GeV – 10 TeV. These constraints appear to prevail over the IB, IA, IC and synchrotron constraints at the high-energy part of the spectrum. In the same spirit as before, we adopt the DR model, and obtain fairly conservative constraints for the entire energy spectrum. The results are presented in Fig. 2 (red line).

Much like the photon-emission response functions, the positron-flux response functions are sensitive to the adopted propagation model, which determines the diffusion and reacceleration of the injected positrons. However, they are insensitive to the DM halo profile, since most of the positrons come from the local region,  $\sim 1$  kpc from the Sun [5]<sup>5</sup>.

#### B. Decay into neutrinos.

Neutrinos are the least detectable stable SM particles, hence constraints on DM decay (or annihilation) to neutrinos can be used to set conservative but robust lower limits on the DM lifetime (or upper limit on the annihilation cross section) to any SM final state [7]. Palomarez-Ruiz [2, 3] obtained limits on the decay channel  $\chi \rightarrow \nu + \bar{\nu}$ . Here we will adapt the analysis of Refs. [2–4], to constrain the decay channel  $\chi \rightarrow \chi' + \nu + \bar{\nu}$ . This

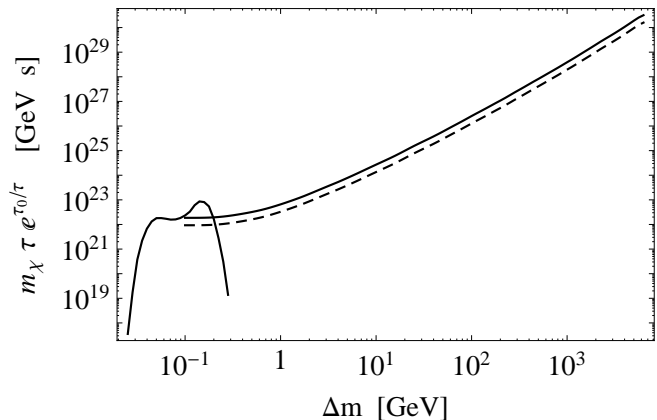


FIG. 3: Limits on dark-matter decay  $\chi \rightarrow \chi' + \nu + \bar{\nu}$ . As in Fig. 2, the solid (dashed) lines correspond to monoenergetic (flat) injection distribution of  $\nu, \bar{\nu}$ . The regions below the lines are excluded.

will set the most conservative limit on DM decay modes of the form  $\chi \rightarrow \chi' + l$ , where  $l$  is any SM final state.

The neutrino flux on Earth from DM decay in the Galactic halo is

$$\frac{d\Phi_\nu}{dE_\nu} = \frac{1}{4\pi} \frac{1}{m_\chi \tau e^{\tau_0/\tau}} \mathcal{J}_{\Delta\Omega} \frac{2}{3} \frac{dN}{dE_\nu} \quad (25)$$

The multiplicity of 2 accounts for the sum of  $\nu$  and  $\bar{\nu}$  produced in the decays. As in Refs. [2, 3], we assume equal decay width to all three neutrino flavors, which accounts for the factor of 1/3 in Eq. (25). This is a reasonable approximation, since neutrino flavor oscillations between the production and detection points will considerably weaken any preference toward a particular flavor. For simplicity, and in order to minimize the uncertainty arising from a particular choice of halo profile, we average the expected neutrino signal over the whole sky,  $\psi = 180^\circ$ . Directional information, whenever available, is in general expected to lead to more stringent limits [2, 3, 8].

For energies  $E_\nu \gtrsim 50$  MeV, the neutrino flux on Earth is dominated by atmospheric neutrinos. The atmospheric neutrino flux has been well measured by a number of experiments [53–58] and is in good agreement with theoretical predictions. We utilize the results of the FLUKA [59, 60] calculation of the atmospheric  $\nu_\mu + \bar{\nu}_\mu$  background, over the energy range 50 MeV to 10 TeV. We determine a DM decay limit by requiring the expected neutrino signal from DM decay not to exceed the atmospheric neutrino flux, integrated over energy bins of width  $\Delta \log_{10} E_\nu \sim 0.3$ . This choice of bin size is in accordance with that adopted in Refs. [2, 3], and encompasses the experimental resolution of the neutrino detectors. (We note that future measurement by IceCube+DeepCore will lead to sensitive limits at high energy [61, 62].)

At low energies  $E_\nu \lesssim 100$  MeV, the relevant data

<sup>5</sup> This is consistent with our assumption in Sec. II A 2, that the  $e^\pm$  do not escape from the inner part of the galaxy.

come from the diffuse supernova neutrino background (DSNB) search performed by the SK experiment [63]. SK searched for positrons produced by incident  $\bar{\nu}_e$  on free protons inside the detector, via the inverse  $\beta$ -decay reaction  $\bar{\nu}_e + p \rightarrow e^+ + n$ . Incoming  $\nu_e$  and  $\bar{\nu}_e$  interact also with bound nucleons, producing electrons and positrons. The main sources of background for these observations are atmospheric  $\nu_e$  and  $\bar{\nu}_e$ , and the Michel electrons and positrons from decays of subthreshold muons. A DSNB signal was not detected. In Refs. [2–4] a  $\chi^2$  analysis of these data was performed, and used to place limits, at 90% confidence level, on the contribution to the signal from DM annihilation,  $\chi\chi \rightarrow \nu\bar{\nu}$ , or decay,  $\chi \rightarrow \nu\bar{\nu}$ . We shall employ the DM decay limits of Refs. [2, 3]. A simple rescaling suffices to convert these limits into constraints on the decay mode of interest here,  $\chi \rightarrow \chi'\nu\bar{\nu}$ , under the assumption that  $\nu\bar{\nu}$  are emitted monoenergetically. The resulting constraints are shown in Fig. 3.

### III. LATE-DECAYING DARK MATTER AND THE SMALL-SCALE GALACTIC STRUCTURE

The standard  $\Lambda$ CDM cosmological model successfully reproduces the observed structure of the Universe at large scales. However, at small scales, there appear to be several inconsistencies between observations and CDM simulations of galaxy formation. The negligible primordial velocity dispersion of CDM particles allows gravitational clustering to occur down to very small scales. Structure forms hierarchically, with small scales collapsing first and forming dense clumps. The resulting phase packing in the inner regions of galaxies leads to cuspy central density profiles [24], which are currently disfavored by the rotational curves of dwarf spheroidal galaxies [22, 23, 25–28]. Dense lumps of matter also survive the mergers and become satellite galaxies. The number of satellite galaxies predicted by CDM simulations greatly exceeds the number observed around the Milky Way [24, 30, 32]. A number of other disparities between observations and CDM predictions have been reported. These include the overestimation of the number of halos in low-density voids [33, 35], the non-prediction of pure-disk or disk-dominated galaxies [29], the large angular-momentum loss by condensing gas [34], and the “bottom-up” hierarchical formation [31].

It is not yet known whether the solution to these inconsistencies lies outside the dark-matter sector. Indeed, individual astrophysical solutions to some of these problems have been suggested. However, it is possible that the apparent discrepancies between CDM and observed galactic structure point toward a modification of the standard CDM scenario. The significance of these hints for deciphering the nature of DM is underscored by the fact that gravitational effects remain the only confirmed evidence for the existence of DM.

A possible alternative to the CDM model is warm dark matter (WDM), whose thermal free-streaming proper-

ties result in a suppression of structure on small scales. Although well-motivated particle-physics candidates for WDM exist, WDM lacks the “naturalness” of the standard CDM scenario in which the observed relic DM abundance arises from thermal freeze-out (CDM candidates produced by other mechanisms also exist). It is possible, though, to incorporate some WDM-like structure-formation features within the CDM paradigm, if we discard the notion that CDM particles are completely stable.

It has been suggested that if the heavy relic particles decay according to Eq.(1), the energy released in the decay will change the standard picture of structure formation. If the decays occur at early times,  $\sim 10^5 \text{ s} - 10^8 \text{ s}$ , before gravitational collapse, the massive decay products acquire non-negligible velocities, which results in a suppression of the amplitude of density perturbations at small scales (still in the linear regime). The daughter DM particles behave effectively as WDM. Existing limits on the free-streaming and phase-packing properties of WDM can be directly translated to determine the interesting and the excluded regions of the CDM decay parameter space [14, 15].

Another interesting possibility, investigated in Refs. [16–19], arises if the decays take place during the nonlinear stages of gravitational collapse. In this scenario the energy acquired by the decay products causes the halo to expand and, as a result, softens the steep central cusps predicted by CDM [16]. It also results in a decrease in the halo circular velocity, which can account for the deficit of satellite galaxies with velocity 10-20 km/s, with respect to standard CDM predictions [17].

The efficacy and viability of the late DM decay mechanism to alleviate the CDM small-scale structure problems depend on two parameters: the parent particle lifetime,  $\tau$ , and the ratio  $\varepsilon \equiv \Delta m/m_\chi$  which gives the recoil velocity of the massive daughter particle,  $v_{\chi'} \simeq \varepsilon$ .<sup>6</sup> Qualitatively, one expects  $\tau$  to be comparable to the age of the Universe, so that the decays occur during galaxy formation. In the limit of very large  $\tau$ , the standard CDM scenario is recovered, while small  $\tau$  corresponds to the early decay scenario, examined in [14, 15]. The velocity imparted to the heavy daughter particles should be sufficiently large – of the order of the virial velocity of the galaxy – in order to have an effect on the formation of the halo. It should not exceed, though, the escape velocity from the halo, which would be catastrophic for the galaxy, unless, of course,  $\tau$  is very large.

Abdelqader and Melia [17] used a semi-analytical approach that allowed them to incorporate the effect of DM decay in halo evolution. They showed that DM

<sup>6</sup> This becomes a strict equality in the case of a 2-body decay. If more than one relativistic particle is produced, as in the cases examined in this paper, the correction in  $v_{\chi'}$  is insignificant.



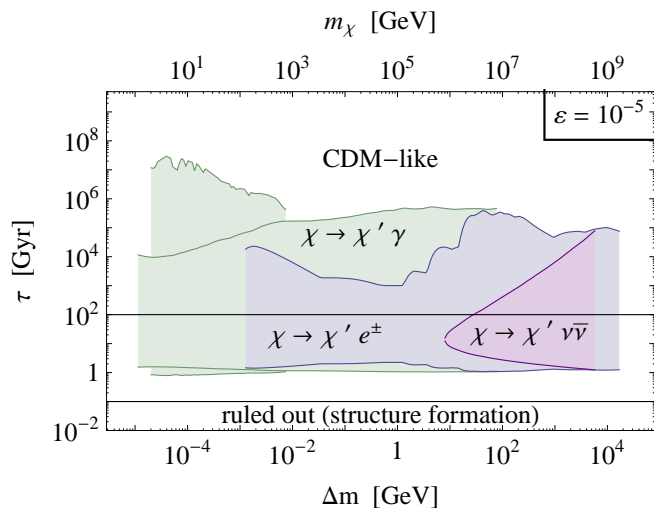


FIG. 4: Constraints on DM lifetime  $\tau$  vs mass splitting  $\Delta m$  and mass  $m_\chi$ , for  $\varepsilon = 10^{-5}$  (recoil velocity  $v_{\chi'} = 5$  km/s), for the decay channels  $\chi \rightarrow \chi' + \gamma$  (green),  $\chi \rightarrow \chi' + e^- + e^+$  (blue) and  $\chi \rightarrow \chi' + \nu + \bar{\nu}$  (purple). Color-shaded regions are excluded by the observed radiation backgrounds (Ref. [1] and this work). The decays may have an observable effect on galactic halo structure if they occur at times  $0.1 \text{ Gyr} < \tau < 100 \text{ Gyr}$  (interval between solid lines). Longer lifetimes  $\tau \gtrsim 100 \text{ Gyr}$  correspond to the standard CDM scenario, while decays occurring at  $\tau \lesssim 0.1 \text{ Gyr}$  (but after the matter-radiation equality) disrupt the galaxy formation significantly and are excluded [18, 19].

decay preferentially heats smaller haloes, causing them to expand, and reduces their present-day circular velocity. They argued that if  $\varepsilon \sim (5 - 7) \times 10^{-5}$  and  $\tau \sim (\text{few} - 30) \text{ Gyr}$ , dark-matter decay can well account for the deficit in the observed number of galaxies with circular velocities in the range 10-20 km/s.

Peter et al. [18, 19] performed a more extensive investigation of the  $\tau - \varepsilon$  parameter space, by means of both semi-analytical calculations and simulations. They demonstrated the way in which DM decay affects the halo mass-concentration relation and mass function, and used measurements of these quantities to constrain the DM decay parameter space. They located the allowed and potentially interesting parameter space roughly within the range

$$\varepsilon = 3.4 \times 10^{-6} - 3.4 \times 10^{-4}, \quad (26)$$

$$\tau = (0.1 - 100) \text{ Gyr}. \quad (27)$$

The corresponding recoil velocity is  $v_{\chi'} = (1 - 100) \text{ km/s}$ . The actual limits on  $\varepsilon$  and  $\tau$  are, of course, correlated.

In Sec. II, we derived constraints on the lifetime for late decay of DM into a massive daughter and either  $e^\pm$  or a  $\nu\bar{\nu}$  pair. For a given value of  $\varepsilon$ , the bounds of Sec. II determine whether these decays can take place in time to affect halo evolution.

The flux of DM decay products in the Galaxy today is proportional to  $1/(m\tau\varepsilon^{\tau_0/\tau})$ , and the limits in Fig.1 are

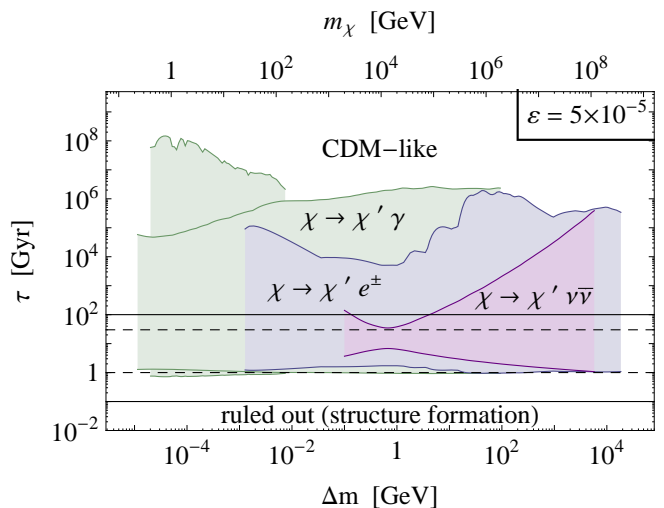


FIG. 5: Same as in Fig. 4, but for  $\varepsilon = 5 \times 10^{-5}$ , or recoil velocity  $v_{\chi'} \simeq 15$  km/s, suggested in [17] as suitable for resolving the missing-satellite problem. This would require a dark-matter lifetime within the narrower interval  $1 \text{ Gyr} < \tau < 30 \text{ Gyr}$  shown (dashed lines).

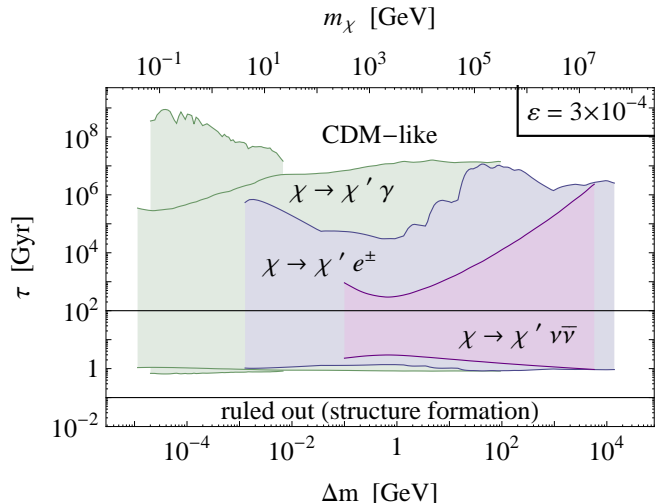


FIG. 6: Same as in Fig. 4, but for  $\varepsilon = 3 \times 10^{-4}$ , or recoil velocity  $v_{\chi'} \simeq 90$  km/s.

expressed in terms of this quantity. Translating these limits to bounds on  $\tau$  alone, we see that the constraints may be satisfied for either (i) very long lifetimes,  $\tau \gg \tau_0$ , for which the current DM decay rate is very small; or (ii) very short lifetimes,  $\tau \ll \tau_0$ , for which the abundance of the unstable parent in the Universe today is very small (as most decays have already taken place). Between these extremes limits lies a band of excluded lifetimes. These bands are shown in Figs. 4 - 6 for three values of  $\varepsilon$  spanning the range given in Eq. (26),  $\varepsilon = 10^{-5}$ ,  $5 \times 10^{-5}$  and  $3 \times 10^{-4}$ , corresponding to recoil velocities  $v_{\chi'} \simeq 5 \text{ km/s}$ ,  $15 \text{ km/s}$ , and  $90 \text{ km/s}$  respectively.

For the values of  $\varepsilon$  considered, the excluded band spans several orders of magnitude in lifetime. These excluded bands become smaller as  $\varepsilon$  is decreased, such that for sufficiently small epsilon there is no constraint. Note that while the upper limit of the excluded band may be improved with more sensitive flux observations, the same is not true for the lower limit, at  $\tau \sim 1$  Gyr, since for these lifetimes the factor  $e^{-\tau_0/\tau}$  dominates. For this reason, the lower limit of the excluded regions for the photon and  $e^\pm$  decay modes are very similar.

We now compare the bounds on the DM lifetime  $\tau$  with the interesting range of values specified in Eq. (27). Figures 4 - 6 show that these bounds significantly constrain, but do not rule out, unstable dark-matter models whose dominant decay channel produces the SM particles considered. For the  $\gamma$  or  $e^\pm$  decay modes, lifetimes greater than  $\sim 1$  Gyr are eliminated, and we thus identify  $\tau \sim (0.1 - 1)$  Gyr as the range of allowed lifetimes for which decays may affect structure formation. For decay modes to neutrinos, however, the allowed lifetimes span the entire interval of Eq. (27) (at least for some masses). Of particular interest, perhaps, is the case of weakly interacting massive particle (WIMP) dark matter of mass  $m_\chi \sim 10^2$  GeV, decaying via the  $\nu\bar{\nu}$  channel, with  $\tau$  and  $\varepsilon$  in accordance with the values suggested in Ref. [17] for resolving the missing satellite problem. These decay parameters are indicated by the dashed lines in Fig. 5.

#### IV. LIMITS ON MODELS WITH LATE DARK-MATTER DECAY

A number of particle-physics models have been proposed which predict or invoke a DM decay mode described by Eq. (1) [64–67]. The motivation for these models varies widely, thus the parameter space of interest does not always overlap with that relevant for structure formation. We now describe, in general terms, when and how the bounds derived in Sec. II can constrain decay modes of the type in Eq. (1). We then apply these considerations to particular models found in recent literature.

In Secs. II and III we assumed that all of the DM was in the form of the heavy, unstable,  $\chi$  particles prior to decay. However, this need not be the case. In fact, many models predict or require that the relic  $\chi$  abundance be only a fraction of the total CDM density. This may be true even if the decay time is larger than the age of the Universe, provided that either (i) other processes (e.g. inelastic scattering) efficiently eliminate the heavy particles ( $\chi$ ) in favor of the light ones ( $\chi'$ ) [65], or (ii) the  $\chi - \chi'$  sector makes only a subdominant contribution to the total DM density. The relic  $\chi$  abundance is, of course, critical in deriving limits on specific models.

Allowing the  $\chi$  abundance to be a free parameter, the four variables which determine the relevance of constraints inferred from the present radiation backgrounds are (i) the mass splitting,  $\Delta m$ , (ii) the mass of the DM

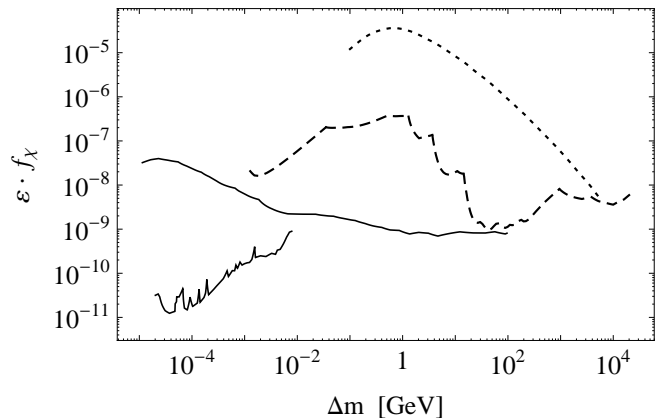


FIG. 7: The observed radiation backgrounds can constrain the lifetime of the heavy DM state only in models which lie in the regions above the lines. Models which lie below the lines cannot be constrained by the bounds presented in Sec. II. As in Fig. 1, the different curves correspond to the decay channels  $\chi \rightarrow \chi' + \gamma$  (solid lines),  $\chi \rightarrow \chi' + e^- + e^+$  (dashed line), and  $\chi \rightarrow \chi' + \nu + \bar{\nu}$  (dotted line).

particle,  $m_\chi$ , or equivalently  $\varepsilon = \Delta m/m_\chi$ , (iii) the decay lifetime of the heavy DM state,  $\tau$ , and (iv) the relic fraction of DM in the form of  $\chi$  particles before decay occurs,  $f_\chi \equiv Y_\chi/Y_{\text{CDM}}$ . In terms of these parameters, the constraints of Sec. II can be expressed as

$$\tau e^{\tau_0/\tau} \geq (\varepsilon \cdot f_\chi) \mathcal{F}(\Delta m)/\Delta m. \quad (28)$$

where  $\mathcal{F}(\Delta m)$  can be read off Fig. 1 for the decay channels considered.

##### A. Fixed $\varepsilon \cdot f_\chi$

Consider constraints on the lifetime for models in which the parameters  $\varepsilon$  and  $f_\chi$  are specified. Similar to the analysis of Sec. III, Eq. (28) implies an excluded band for  $\tau$ , provided that the fraction of energy released per decay (here quantified by  $\varepsilon$ ) and/or the fraction of decaying dark matter,  $f_\chi$ , are sufficiently large. More specifically, in order for Eq. (28) to translate into constraints on  $\tau$ , the parameters  $\varepsilon, f_\chi$  must satisfy

$$\varepsilon \cdot f_\chi \geq \frac{\tau_0 e}{\mathcal{F}(\Delta m)/\Delta m}. \quad (29)$$

(since  $\tau e^{\tau_0/\tau} \geq \tau_0 e$ , for any  $\tau$ ).

In Fig. 7 we sketch the regions defined by Eq. (29), for the three decay channels under consideration. Models which lie above (below) the curves are constrained (not constrained) by the bounds derived in Sec. II using the observed radiation backgrounds. For models that lie on the curves, the constraint (28) produces a zero-width exclusion band for the lifetime at  $\tau = \tau_0$ . Larger values of  $\varepsilon \cdot f_\chi$  yield exclusion bands which span a range of lifetimes around  $\tau_0$ .

The above discussion is relevant to a class of models proposed in Refs. [64, 65], in which DM possesses an excited state. As a result of an approximate symmetry, the excited state is separated by a small mass splitting from the ground state, to which it decays with emission of  $e^\pm$  pairs. For a particular implementation of these models, with  $\Delta m \approx 2$  MeV and  $m_\chi \approx 500$  GeV, the kinetic excitations and the subsequent decays of DM particles inside the Galactic halo can produce the positrons which give rise to the observed 511 keV annihilation line in the center of our Galaxy [64]. For the range of parameters favored by the 511 keV signal,  $f_\chi \lesssim 10^{-3}$  and  $\varepsilon \simeq 10^{-7} - 10^{-6}$ , the scenario lies comfortably below the  $e^\pm$  curve in Fig. 7, and is thus not constrained by our observational bounds. However, significantly larger values of  $\varepsilon \cdot f_\chi$  are possible within the same generic class of models, for which our bounds would impose a non-trivial constraint.

### B. Fixed $\tau$

Returning to the constraint of Eq. (28), we now consider models in which  $\tau$  (rather than  $\varepsilon \cdot f_\chi$ ) is narrowly specified. Equation (28) then limits the energy release via decay, and relic abundance of the unstable state, as per

$$\varepsilon \cdot f_\chi \leq \frac{\tau e^{\tau_0/\tau}}{\mathcal{F}(\Delta m)/\Delta m}. \quad (30)$$

This constraint is substantial only if

$$\tau e^{\tau_0/\tau} \leq \mathcal{F}(\Delta m)/\Delta m \quad (31)$$

(since by definition  $\varepsilon, f_\chi \leq 1$ ). We obtain a nontrivial constraint provided that  $1 \text{ Gyr} \lesssim \tau \lesssim 10^6 - 10^{12} \text{ Gyr}$ , where the exact range depends on the mass splitting and the decay channel considered. Models with  $\tau \lesssim 1 \text{ Gyr}$  trivially satisfy the bounds placed by radiation backgrounds, as do models with very large  $\tau$ , in accordance with the discussion in Sec. III.

The “degenerate gravitino” scenario of Ref. [67] falls in the category of models whose energy release may be constrained by observations. In this scenario, the lightest supersymmetric particle (LSP) and the next-to-lightest supersymmetric particle (NLSP) have a small mass splitting,  $\Delta m \sim 10^{-2}$  GeV, such that the slightly heavier NLSP can decay into the LSP with emission of a photon, with a lifetime comparable to the age of the Universe. These parameters satisfy the inequality (31) and thus the observational bounds represent a non-trivial constraint on the model. Specifically, the photon bounds [1] constrain the relic NLSP abundance before decay in a mixed (NLSP + LSP) DM scenario, as explicitly shown in Ref. [67].

As an example of models which trivially evade the constraint (30), we mention here the inelastic DM scenarios [66]. These models aim to reconcile the results

of DAMA and CDMS direct detection experiments, by evoking small mass splittings  $\Delta m \sim 100$  keV. However, since the decays occur very early (before recombination) this scenario cannot be constrained by the present radiation backgrounds. Substituting the lifetime of the heavier state  $\tau \sim (10^2 - 10^3) \text{ yr}$  into Eq. (31) of course trivially verifies this fact.

## V. CONCLUSIONS

The decay lifetime is a fundamental property of dark matter. Knowledge of this parameter may provide an essential clue for unravelling the particle nature of dark matter. In the standard CDM scenario, dark matter particle interactions play no role in the evolution of the Universe subsequent to DM freeze-out, which limits our ability to probe DM particle interactions via cosmological observations. However, there is a large class of DM models in which DM particle interactions are in fact invoked to explain cosmological observations. One such hypothesis is that DM decay may provide a possible solution to the small scale structure problems of standard CDM.

We have considered a class of DM models in which DM decays at late times to a nearly degenerate daughter plus relativistic particles,  $\chi \rightarrow \chi' + l$ . In this scenario, the relativistic daughters carry only a small fraction,  $\varepsilon = \Delta m/m_\chi$ , of the parent DM mass and thus decays do not alter the DM energy density. However, the energy acquired by the daughter  $\chi'$  effectively heats the halo, and has been proposed as a means of modifying halo structure in such a way as to bring CDM predictions into better agreement with observation.

We focused on the scenario in which the relativistic daughters consist of Standard Model particles, and derived constraints on the cases in which those daughter particles are either  $e^\pm$  or neutrinos. In Fig. 1 we summarize these constraints and compare them with the analogous photon bounds obtained in Ref. [1]. Since photons provide the most stringent bounds and neutrinos the least stringent, these results, taken together, delineate the range of lifetime bounds for these models.

Our constraints on the  $e^\pm$  decay mode lie between those for photons and neutrinos, though we note that there are some masses for which the  $e^\pm$  constraints become comparable to those for photons. Note that many models that allow the process  $\chi \rightarrow \chi' \bar{\nu} \nu$  will also allow  $\chi \rightarrow \chi' e^+ e^-$ , for which stronger bounds apply.

For the  $e^\pm$  (and  $\gamma$ ) decay modes, the lifetime must either be much greater than the age of the Universe (for which decay cannot affect structure formation) or smaller than  $\sim 1 \text{ Gyr}$ . Though this eliminates some of the parameter space of interest in structure evolution, a significant portion remains open. For the  $\bar{\nu} \nu$  decay modes, a much larger range of lifetimes is permitted.

Models which are not necessarily motivated by structure formation considerations, but nonetheless entail decay between particle states of similar mass, may also be

constrained by the bounds presented here. This is possible, provided that the relic density of the heavier state from the early Universe is not too small, and/or the decay lifetime is larger than 1 Gyr. The constraints and the analysis presented here can provide generic useful guidelines for constructing models which feature decay modes between closely degenerate states.

We note that our limits in Figs. 1 - 3 are strictly applicable only for  $\varepsilon \ll 1$  (so that the approximation  $E_l \simeq \Delta m$  is valid). However, for  $\varepsilon = 1$ , our monoenergetic constraints correspond to those for the decays  $\chi \rightarrow e^+e^-$  and  $\chi \rightarrow \bar{\nu}\nu$  (i.e., where there is no  $\chi'$ ). For the  $\bar{\nu}\nu$  case this simply reproduces the results of Ref. [2]. For the  $e^\pm$  case, our bounds inferred using inverse Compton scattering and bremsstrahlung emission, synchrotron radiation, and

the positron flux, reproduce the ones derived in Ref. [10], using the same response functions employed here. However, the monoenergetic limits of Fig. 2 inferred from the in-flight and at-rest annihilations represent strong new constraints of general applicability for the decay mode  $\chi \rightarrow e^+e^-$ , in the interval  $2 \text{ MeV} \lesssim m_{\text{DM}} \lesssim 1 \text{ GeV}$ .

### Acknowledgements

NFB and KP were supported, in part, by the Australian Research Council, and AJG by the Commonwealth of Australia. We thank F. Melia, J. Beacom and H. Yüksel for useful discussions.

- 
- [1] H. Yüksel and M. D. Kistler, *Phys. Rev.* **D78**, 023502 (2008), arXiv:0711.2906.
- [2] S. Palomares-Ruiz, *Phys. Lett.* **B665**, 50 (2008), arXiv:0712.1937.
- [3] S. Palomares-Ruiz, (2008), arXiv:0805.3367.
- [4] S. Palomares-Ruiz and S. Pascoli, *Phys. Rev.* **D77**, 025025 (2008), arXiv:0710.5420.
- [5] L. Zhang, G. Sigl, and J. Redondo, *JCAP* **0909**, 012 (2009), arXiv:0905.4952.
- [6] L. Zhang, C. Weniger, L. Maccione, J. Redondo, and G. Sigl, (2009), arXiv:0912.4504.
- [7] J. F. Beacom, N. F. Bell, and G. D. Mack, *Phys. Rev. Lett.* **99**, 231301 (2007), arXiv:astro-ph/0608090.
- [8] H. Yüksel, S. Horiuchi, J. F. Beacom, and S. Ando, *Phys. Rev.* **D76**, 123506 (2007), arXiv:0707.0196.
- [9] N. F. Bell and T. D. Jacques, *Phys. Rev.* **D79**, 043507 (2009), arXiv:0811.0821.
- [10] M. Cirelli, P. Panci, and P. D. Serpico, (2009), arXiv:0912.0663.
- [11] The Fermi-LAT Collaboration, (2010), arXiv:1002.2239.
- [12] G. D. Mack, T. D. Jacques, J. F. Beacom, N. F. Bell, and H. Yüksel, *Phys. Rev.* **D78**, 063542 (2008), arXiv:0803.0157.
- [13] R. M. Crocker, N. F. Bell, C. Balazs, and D. I. Jones, *Phys. Rev.* **D81**, 063516 (2010), arXiv:1002.0229.
- [14] J. A. R. Cembranos, J. L. Feng, A. Rajaraman, and F. Takayama, *Phys. Rev. Lett.* **95**, 181301 (2005), arXiv:hep-ph/0507150.
- [15] M. Kaplinghat, *Phys. Rev.* **D72**, 063510 (2005), arXiv:astro-ph/0507300.
- [16] F. J. Sanchez-Salcedo, *Astrophys. J.* **591**, L107 (2003), arXiv:astro-ph/0305496.
- [17] M. Abdelqader and F. Melia, *Mon. Not. Roy. Astron. Soc.* **388**, 1869 (2008), arXiv:0806.0602.
- [18] A. H. G. Peter, *Phys. Rev.* **D81**, 083511 (2010), arXiv:1001.3870.
- [19] A. H. G. Peter, C. E. Moody, and M. Kamionkowski, *Phys. Rev.* **D81**, 103501 (2010), arXiv:1003.0419.
- [20] R. Cen, *Astrophys. J.* **546**, L77 (2001), arXiv:astro-ph/0005206.
- [21] K. Ichiki, M. Oguri, and K. Takahashi, *Phys. Rev. Lett.* **93**, 071302 (2004), arXiv:astro-ph/0403164.
- [22] G. Gentile, P. Salucci, U. Klein, D. Vergani, and P. Kalberla, *Mon. Not. Roy. Astron. Soc.* **351**, 903 (2004), arXiv:astro-ph/0403154.
- [23] P. Salucci *et al.*, *Mon. Not. Roy. Astron. Soc.* **378**, 41 (2007), arXiv:astro-ph/0703115.
- [24] J. Diemand, M. Kuhlen, and P. Madau, *Astrophys. J.* **657**, 262 (2007), arXiv:astro-ph/0611370.
- [25] G. Gilmore *et al.*, *Nucl. Phys. Proc. Suppl.* **173**, 15 (2007), arXiv:astro-ph/0608528.
- [26] G. Gilmore *et al.*, *Astrophys. J.* **663**, 948 (2007), arXiv:astro-ph/0703308.
- [27] G. Gilmore *et al.*, (2008), arXiv:0804.1919.
- [28] R. F. G. Wyse and G. Gilmore, (2007), arXiv:0708.1492.
- [29] F. Governato *et al.*, *Astrophys. J.* **607**, 688 (2004), arXiv:astro-ph/0207044.
- [30] A. A. Klypin, A. V. Kravtsov, O. Valenzuela, and F. Prada, *Astrophys. J.* **522**, 82 (1999), arXiv:astro-ph/9901240.
- [31] N. Metcalfe, T. Shanks, A. Campos, H. J. McCracken, and R. Fong, *Mon. Not. Roy. Astron. Soc.* **323**, 795 (2001), arXiv:astro-ph/0010153.
- [32] B. Moore *et al.*, *Astrophys. J.* **524**, L19 (1999).
- [33] P. J. E. Peebles, *Astrophys. J.* **557**, 495 (2001), arXiv:astro-ph/0101127.
- [34] J. Sommer-Larsen and A. Dolgov, *Astrophys. J.* **551**, 608 (2001), arXiv:astro-ph/9912166.
- [35] A. V. Tikhonov, S. Gottloeber, G. Yepes, and Y. Hoffman, (2009), arXiv:0904.0175.
- [36] J. F. Navarro, C. S. Frenk, and S. D. M. White, *Astrophys. J.* **462**, 563 (1996), arXiv:astro-ph/9508025.
- [37] J. F. Beacom, N. F. Bell, and G. Bertone, *Phys. Rev. Lett.* **94**, 171301 (2005), arXiv:astro-ph/0409403.
- [38] J. Mardon, Y. Nomura, D. Stolarski, and J. Thaler, *JCAP* **0905**, 016 (2009), arXiv:0901.2926.
- [39] A. W. Strong, H. Bloemen, R. Diehl, W. Hermsen, and V. Schoenfelder, *Astrophys. Lett. Commun.* **39**, 209 (1999), arXiv:astro-ph/9811211.
- [40] S. D. Hunter *et al.*, *Astrophys. J.* **481**, 205 (1997).
- [41] J. F. Beacom and H. Yüksel, *Phys. Rev. Lett.* **97**, 071102 (2006), arXiv:astro-ph/0512411.
- [42] A. W. Strong and I. V. Moskalenko, *Astrophys. J.* **509**, 212 (1998), arXiv:astro-ph/9807150.
- [43] P. A. M. Dirac, *Proc. Camb. Phil. Soc.* **26**, 361 (1930).
- [44] P. Sizun, M. Casse, and S. Schanne, *Phys. Rev.* **D74**,

- 063514 (2006), arXiv:astro-ph/0607374.
- [45] N. Prantzos, *Astron. Astrophys.* **449**, 869 (2006), arXiv:astro-ph/0511190.
- [46] F. W. Stecker, *Astrophys. Space Sci.* **3**, 579 (1969).
- [47] P. Jean *et al.*, *Astron. Astrophys.* **445**, 579 (2006), arXiv:astro-ph/0509298.
- [48] J. Knodlseder *et al.*, *Astron. Astrophys.* **441**, 513 (2005), arXiv:astro-ph/0506026.
- [49] G. Dobler, D. P. Finkbeiner, I. Cholis, T. R. Slatyer, and N. Weiner, (2009), arXiv:0910.4583.
- [50] C.-R. Chen, S. K. Mandal, and F. Takahashi, *JCAP* **1001**, 023 (2010), arXiv:0910.2639.
- [51] PAMELA, O. Adriani *et al.*, *Nature* **458**, 607 (2009), arXiv:0810.4995.
- [52] The Fermi LAT collaboration, A. A. Abdo *et al.*, *Phys. Rev. Lett.* **102**, 181101 (2009), arXiv:0905.0025.
- [53] Super-Kamiokande, Y. Ashie *et al.*, *Phys. Rev.* **D71**, 112005 (2005), arXiv:hep-ex/0501064.
- [54] Frejus., K. Daum *et al.*, *Z. Phys.* **C66**, 417 (1995).
- [55] The AMANDA Collaboration, J. Ahrens *et al.*, *Phys. Rev.* **D66**, 012005 (2002), arXiv:astro-ph/0205109.
- [56] The IceCube Collaboration, (2007), arXiv:0711.0353.
- [57] MACRO, M. Ambrosio *et al.*, *Eur. Phys. J.* **C36**, 323 (2004).
- [58] Soudan-2, W. W. M. Allison *et al.*, *Phys. Rev.* **D72**, 052005 (2005), arXiv:hep-ex/0507068.
- [59] G. Battistoni, A. Ferrari, T. Montaruli, and P. R. Sala, *Astroparticle Physics* **19**, 269 (2003).
- [60] G. Battistoni, A. Ferrari, T. Montaruli, and P. R. Sala, (2003), arXiv:hep-ph/0305208.
- [61] S. K. Mandal, M. R. Buckley, K. Freese, D. Spolyar, and H. Murayama, *Phys. Rev.* **D81**, 043508 (2010), arXiv:0911.5188.
- [62] M. R. Buckley, K. Freese, D. Hooper, D. Spolyar, and H. Murayama, *Phys. Rev.* **D81**, 016006 (2010), arXiv:0907.2385.
- [63] Super-Kamiokande, M. Malek *et al.*, *Phys. Rev. Lett.* **90**, 061101 (2003), arXiv:hep-ex/0209028.
- [64] D. P. Finkbeiner and N. Weiner, *Phys. Rev.* **D76**, 083519 (2007), arXiv:astro-ph/0702587.
- [65] D. P. Finkbeiner, N. Padmanabhan, and N. Weiner, *Phys. Rev.* **D78**, 063530 (2008), arXiv:0805.3531.
- [66] D. Tucker-Smith and N. Weiner, *Phys. Rev.* **D64**, 043502 (2001), arXiv:hep-ph/0101138.
- [67] L. Boubekour, K. Y. Choi, R. R. de Austri, and O. Vives, *JCAP* **1004**, 005 (2010), arXiv:1002.0340.